

Recognizing critical lines via entanglement in non-Hermitian systems

Keshav Das Agarwal, Tanoy Kanti Konar, Leela Ganesh Chandra Lakkaraju, Aditi Sen(De)
Harish-Chandra Research Institute, A CI of Homi Bhabha National Institute, Chhatmag Road, Jhansi, Allahabad - 211019, India

The non-Hermitian model exhibits counter-intuitive phenomena which are not observed in the Hermitian counterparts. To probe the competition between non-Hermitian and Hermitian interacting components of the Hamiltonian, we focus on a system containing non-Hermitian XY spin chain and Hermitian Kaplan-Shekhtman-Entin-Aharony (KSEA) interactions along with the transverse magnetic field. We show that the non-Hermitian model can be an effective Hamiltonian of a Hermitian XX spin- $\frac{1}{2}$ with KSEA interaction and a local magnetic field that interacts with local and non-local reservoirs. The analytical expression of the energy spectrum divides the system parameters into two regimes – in one region, the strength of Hermitian KSEA interactions dominates over the imaginary non-Hermiticity parameter while in the other, the opposite is true. In the former situation, we demonstrate that the nearest-neighbor entanglement and its derivative can identify quantum critical lines with the variation of the magnetic field. In this domain, we determine a surface where the entanglement vanishes, similar to the factorization surface, known in the Hermitian case. On the other hand, when non-Hermiticity parameters dominate, we report the exceptional and critical points where the energy gap vanishes and illustrate that bipartite entanglement is capable of detecting these transitions as well. Going beyond this scenario, when the ground state evolves after a sudden quench with the transverse magnetic field, both rate function and the fluctuation of bipartite entanglement quantified via its second moment can detect critical lines generated without quenching dynamics.

I. INTRODUCTION

Non-Hermitian quantum systems provide a fresh perspective on traditionally established concepts in the Hermitian domain such as quantum phase transitions, topological phases, and the role of symmetry in quantum mechanics [1–3]. For almost two decades or so, investigations of such systems have generated lots of interest since effective non-Hermitian systems can be obtained by dilating the system in a larger Hermitian system [4] or by introducing skew Hermitian part in the dynamics of a state which include gain and loss of energy or particles [5, 6]. Moreover, when the system is in contact with a noisy environment, the evolution of the system, in the weak coupling limit, is well described by the Gorini–Kossakowski–Lindblad–Sudarshan (GKLS) [7, 8] master equation involving Lindblad operators which leads to non-Hermitian Hamiltonian [9–12] and quantum jump operators realized by the continuous measurement performed on the system by the environment [13, 14]. Further, the spectacular experimental developments in several physical platforms like photonics [15], and superconducting systems [16] promise to realize such non-Hermitian systems in a controlled manner. As a result, various suggestions for quantum technologies, such as quantum thermal machines [10, 17], and quantum sensors [18–24] that exploit non-Hermiticity in systems, have been developed in recent years.

In this work, we concentrate on non-Hermitian Hamiltonian which is an effective Hamiltonian in the framework of open quantum systems through the quantum trajectory method without quantum jump operators [13, 14, 25, 26]. Such systems possess exceptional points (EPs) where the corresponding Hamiltonian becomes defective due to the coalescence of eigenvectors [27–29] (see Refs. [11, 29] for Liouvillian EPs). It was shown that the EPs of the non-Hermitian Hamiltonian with parity-time reversal symmetry (\mathcal{PT} -symmetry) can divide the parameter space into two phases – unbroken phase with real eigenspectrum which can be mapped to a Hermitian

Hamiltonian [30, 31], and the broken region having complex eigenvalues. The presence of non-Hermiticity can often result in counter-intuitive behaviors such as localization-delocalization phenomena [32, 33], dynamical quantum phase transitions (DQPT) [34–49] in non-Hermitian lattices [50], gapless phases in p-wave superconductors exhibiting interesting features in dynamics [50–53], multiparty entanglement in the Lipkin-Meshkov-Glick model [54], quantum phase transition in the dissipative Ising chain [55, 56], and mode entanglement between fermions differentiating between non-trivial and trivial phases of topological materials [57–61].

In recent years, the broken-to-unbroken transition of non-Hermitian quantum spin models was studied in which the non-Hermiticity is inserted either in the interaction part by making imaginary coupling constant or by taking the imaginary strength of the magnetic field in the Hamiltonian [62–65]. In this paper, we focus on an interacting quantum spin model which can activate a competition between Hermitian and non-Hermitian interaction terms. In particular, we introduce a rotational and time-reversal symmetric system consisting of non-Hermitian interaction parts in the xy -plane having a imaginary non-Hermiticity constant, representing iXY model and a Hermitian Kaplan-Shekhtman-Entin-Aharony interaction (KSEA) [66–68] in presence of a magnetic field in the z -direction. First, we demonstrate that such a non-Hermitian Hamiltonian is an effective description of a spin chain with XX and KSEA interactions having transverse magnetic field attached to a local and non-local bath, which can be achieved by manipulating the baths [69, 70]. Moreover, the Hamiltonian can be mapped to a quadratic free fermionic model using the Jordan-Wigner transformation [71–74] and hence the behavior of several physical quantities including energy, classical correlators, and bipartite entanglement can be investigated both for finite-size systems consisting of a large number of sites and in the thermodynamic limit.

We indeed observe a trade-off relation between imaginary non-Hermiticity parameters and interaction strength of

KSEA. Specifically, we exhibit that the entire analysis can be divided into two distinct regions – in one region, the strength of the KSEA interaction is slightly higher than the non-Hermiticity parameter present in the iXY part; in the other domain, the non-Hermiticity parameter rules over the KSEA interaction strength, thereby increasing non-Hermiticity component in the system. In the former case, an entire unbroken region emerges where the system mimics the properties of a Hermitian Hamiltonian, known as \mathcal{RT} -symmetry-protected region. In particular, the model in this case contains two striking features – quantum critical point obtained by tuning the strength of the magnetic field where the energy gap vanishes and the factorization surface where the entanglement vanishes. We report that the entanglement pattern, especially the derivative of nearest-neighbor entanglement can capture both critical points and factorization surfaces. Moreover, we show that by gauge transformation in the fermionic basis, the non-Hermitian model having both XY and KSEA interactions can be transformed into the Hermitian XY model having factorization surface known in literature [75, 76] which matches with the factorization surface found in the non-Hermitian counterparts. In the case when non-Hermiticity dominates, we analytically determine that the system possesses an exceptional point, separating broken phase from the unbroken one and also quantum critical points having vanishing gap from the expression of the energy spectrum. By carefully defining the right eigenvector having the lowest imaginary eigenvalue, we demonstrate that the derivative of nearest-neighbor entanglement of the ground state can show non-analyticity around the exceptional point as well as at the critical point with respect to the magnetic field. It establishes that bipartite entanglement can capture aspects that are solely present in the non-Hermitian model as well as critical points connected to gap-closing.

As non-Hermitian systems typically arise in non-equilibrium situations, it is interesting to probe the system with a sudden quench [77]. Initially, the system is prepared in the ground state of the unbroken region and is then quenched in various parameter regimes, especially across the critical points based on gap-closing. Specifically, we illustrate that when the quenching is across the critical point, i.e., the initial magnetic field is much stronger than the strength of the final magnetic field and vice-versa, the conventional dynamical quantity like the rate function based on the overlap of the initial and the evolved states shows non-analyticity with time, thereby detecting the quantum critical point. However, there are situations when both the magnetic fields are weak, the rate function can give the incorrect signal of the quantum critical point. In addition to the rate function, we examine the dynamics of nearest-neighbor entanglement, quantified by its second moment and determine that it is capable of identifying critical points in the system.

The organization of the paper is as follows. In Sec. II, we introduce the model having iXY and KSEA interactions along with magnetic field and provide the Hermitian model which leads to its effective description. In Sec. II A, we analytically derive the exceptional point and establish its connection with the factorization surface of the corresponding

Hermitian model. We demonstrate the capability of nearest-neighbor entanglement in detecting critical points present in this model in Sec. III. In Sec. IV, by performing sudden quench of the ground state in different parameter regimes, the dynamical states are studied with the help of Loschmidt echo, and the corresponding rate function as well as via nearest-neighbor entanglement in Secs. IV A and IV B respectively. Finally, we conclude in Sec. V.

II. EFFECTIVE NON-HERMITIAN HAMILTONIAN

In general, non-Hermiticity in a quantum system can be attributed to two different scenarios - (1) continuous measurement on the system, and (2) the system undergoing dissipative dynamics due to the interaction with the environment which can effectively be described by a non-Hermitian Hamiltonian. These kinds of non-Hermitian Hamiltonian are useful as they possess real eigenvalues, known as pseudo-Hermitian models, having some symmetry. Such quintessential examples of anti-unitary symmetries which bestow a Hamiltonian with real eigenvalues are \mathcal{PT} and \mathcal{RT} -symmetries, where \mathcal{P} , \mathcal{R} and \mathcal{T} stands for parity, rotation and time reversal operation respectively. A region containing a set of parameters in the system having imaginary energy spectrum is called broken while tuning a set of parameters leads to a real spectrum in a non-Hermitian model, known as the unbroken phase. The transition from broken to the unbroken region by varying system parameters occurs around a transition point, referred to as an exceptional point which plays a crucial role in quantum metrology, thermal engines, and many more [3, 10, 23].

In this paper, we focus on \mathcal{RT} -symmetric Hamiltonian where $\mathcal{R} \equiv \exp\left[-i\frac{\pi}{4}\sum_{j=1}^N\sigma_j^z\right]$, a $\frac{\pi}{2}$ rotation around the z -axis and the time-reversal operation, $\mathcal{T}i\mathcal{T}^{-1} = -i$. Although the Hamiltonian satisfies the relation, $[H, \mathcal{RT}] = 0$, due to the anti-unitary properties of the symmetry operations in the broken region, eigenstates of the Hamiltonian do not have \mathcal{RT} symmetry. Let us describe how the non-Hermitian Hamiltonian containing imaginary interaction strength described below can be written as an effective description of a system evolving and interacting with an engineered reservoir. Notice that an effective Hamiltonian undergoing continuous monitoring or measurements can be shown to represent a non-Hermitian system in the presence of imaginary magnetic field having \mathcal{P} and \mathcal{T} symmetry [78].

We consider a one-dimensional spin model of N spin- $\frac{1}{2}$ particles with nearest-neighbor interactions, governed by the Hamiltonian described as,

$$H_S = J \sum_j (\sigma_j^x \sigma_{j+1}^x + \sigma_j^y \sigma_{j+1}^y) + \frac{h'}{2} \sigma_j^z + \frac{K'}{4} (\sigma_j^x \sigma_{j+1}^y + \sigma_j^y \sigma_{j+1}^x) \quad (1)$$

where σ^α ($\alpha = x, y, z$) denotes the Pauli matrix with the periodic boundary being imposed, $\sigma_{N+1} = \sigma_1$, the first two interacting terms represent the XX interaction, $\frac{h'}{J} = h$ is

the strength of the transverse magnetic field, and $\frac{K'}{J} = K$ is the coupling parameter of the symmetric helical interaction, called Kaplan-Shekhtman-Entin-Aharony interaction [66–68] which is found in solid-state materials such as $Ba_2CuGe_2O_7$ and Yb_4As_3 [79]. Reservoir engineering has been instrumental in many phenomena such as nonreciprocal photon transmission [69] and persistent currents in the system [80]. Suppose every individual spin is attached to a local bath while each nearest-neighbor spin pair is attached to a common non-local bath (see schematic representation of the set up in Fig. 1). In this scenario, the evolution of the system interacting with an engineered reservoir is governed by the GKLS master equation [7], given by

$$\frac{d\rho}{dt} = -i[H_S, \rho] + \kappa \sum_j \mathcal{L}[\sigma_j^-](\rho) + \sum_j \mathcal{L}[g_j(\{\sigma\})](\rho), \quad (2)$$

where $\mathcal{L}[A]$ are a set of operators, effectively describing the effects of the environment on the system, known as the Lindblad operators. Note that the second term represents the local dissipation of strength κ and the third term is present due to non-local dissipation between the sites, given by g_j [80]. The action of such superoperator is given mathematically as $\mathcal{L}[A] = A\rho A^\dagger - \frac{1}{2}\{A^\dagger A, \rho\}$ and

$$g_j(\{\sigma\}) = p\sigma_j^- + q\sigma_j^+ + r\sigma_{j+1}^- + s\sigma_{j+1}^+, \quad (3)$$

where p, q, r and s denote the suitable coupling parameters with the correlated environment which can, in general, be complex. In order to arrive at a \mathcal{RT} -symmetric Hamiltonian, we choose $p, s = 0$, $q = -\gamma/\sqrt{2}$ and $r = \gamma/\sqrt{2}$ and Eq. (3) reduces to

$$\frac{d\rho}{dt} = -i(H_{eff}\rho - \rho H_{eff}^\dagger) + \sum_j \mathcal{L}[A_j]\rho\mathcal{L}[A_j]^\dagger,$$

where $H_{eff} = (H_S - \frac{i}{2}\sum_j \mathcal{L}[A_j]^\dagger\mathcal{L}[A_j])$ is the effective Hamiltonian which is non-Hermitian and $\sum_j \mathcal{L}[A_j]\rho\mathcal{L}[A_j]^\dagger$ is called jump operation. In the semi-classical limit, neglecting the jump operation, the evolution of the system can be shown to govern by the non-Hermitian Hamiltonian. Hence the effective Hamiltonian is given by

$$\begin{aligned} H_{eff} &= H_S - \frac{i}{2} \sum_{j=1}^N \mathcal{L}[g_j(\{\sigma\})]^\dagger \mathcal{L}[g_j(\{\sigma\})] \\ &= H_S - \frac{i\gamma}{4} \sum_{j=1}^N (\sigma_j^+ - \sigma_{j+1}^-)(\sigma_j^- - \sigma_{j+1}^+) \\ &= \sum_{j=1}^N \left(h + \frac{i\gamma}{4} \right) \sigma_j^z + \frac{1}{4} \left((1+i\gamma)\sigma_j^x\sigma_{j+1}^x \right. \\ &\quad \left. + (1-i\gamma)\sigma_j^y\sigma_{j+1}^y \right) + \frac{K}{4} (\sigma_j^x\sigma_{j+1}^y + \sigma_j^y\sigma_{j+1}^x). \end{aligned} \quad (4)$$

Notice that there are two-imaginary terms present, one in the coupling and another one in the magnetic field, in the Hamiltonian, thereby making it non-Hermitian. By modifying local

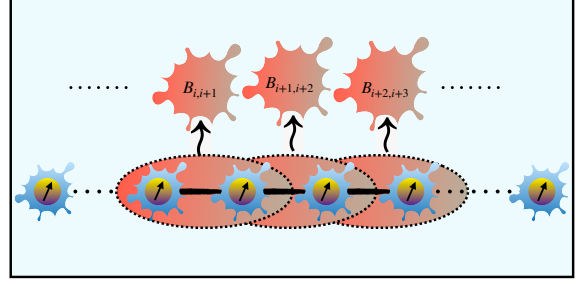


FIG. 1. Schematic representation of the effective non-Hermitian Hamiltonian. When the XX model with KSEA interactions between neighboring sites and transverse magnetic fields are in contact with local and non-local baths, the dynamics can be governed by the effective non-Hermitian model, studied in this work. It leads to a possible method to realize this Hamiltonian in laboratories.

dissipative environment strength κ in Eq. (2), the imaginary part of the magnetic field can be made vanishing, so that the effective Hamiltonian only contains the imaginary part in the coupling, leading to [81]

$$\begin{aligned} H^{iKSEA} &= \sum_j \frac{(1+i\gamma)}{4} \sigma_j^x\sigma_{j+1}^x + \frac{(1-i\gamma)}{4} \sigma_j^y\sigma_{j+1}^y \\ &\quad + \frac{K}{4} (\sigma_j^x\sigma_{j+1}^y + \sigma_j^y\sigma_{j+1}^x) + \frac{h}{2} \sigma_j^z, \end{aligned} \quad (5)$$

with γ being the non-Hermiticity parameter. We will illustrate that the above non-Hermitian system possesses some rich properties which we will reveal with and without quenching dynamics.

A. Exceptional point and connection with factorization point

In order to describe distinctive features of H^{iKSEA} , we need to identify the exceptional point which can be obtained by evaluating the dispersion relation for the non-Hermitian Hamiltonian [62]. By applying the Jordan-Wigner transformation (JW), the model reduces to a free-fermionic Hamiltonian given by,

$$\begin{aligned} H_{JW}^{iKSEA} &= \frac{1}{2} \sum_j (c_j^\dagger c_{j+1} + c_{j+1}^\dagger c_j) + i(\gamma - K)c_j^\dagger c_{j+1}^\dagger \\ &\quad + i(\gamma + K)c_{j+1}c_j + h(2c_j^\dagger c_j - 1), \end{aligned} \quad (6)$$

where c_j^\dagger and c_j represent fermionic creation and annihilation operators, following $\{c_i, c_j^\dagger\} = \delta_{ij}$. The above model is also known as the Kitaev model with imbalanced pairing, with exotic topological properties [57, 82]. Let us perform the second step involving Fourier transformation which transforms

the fermionic operators into their conjugate momentum as

$$c_j = \frac{1}{\sqrt{N}} \sum_{p=-N/2}^{N/2} \exp\left(-\frac{2\pi j p}{N}\right) a_p,$$

and $c_j^\dagger = \frac{1}{\sqrt{N}} \sum_{p=-N/2}^{N/2} \exp\left(\frac{2\pi j p}{N}\right) a_p^\dagger.$ (7)

Due to the periodic boundary condition, the system possesses translational invariance, such that the momentum is a good quantum number which allows the Hamiltonian to be decomposed into the individual momentum sectors, described by $H_{JW}^{iKSEA} = \oplus H_p^{iKSEA}$. Therefore, Eq. (6) reduces to

$$\begin{aligned} \bar{H}_p^{iKSEA} = & \sum_{p>0} (h + \cos \phi_p) (a_p^\dagger a_p + a_{-p}^\dagger a_{-p}) \\ & + \sin \phi_p [(\gamma - K) a_p^\dagger a_{-p}^\dagger + (\gamma + K) a_p a_{-p}] - h, \end{aligned}$$

where $\phi_p = (2p - 1)\pi/N$ and $p \in 1, \dots, N/2$ as we choose anti-periodic boundary condition, $c_{N+1} = -c_1$ [83]. In thermodynamic limit, i.e., $N \rightarrow \infty$, the momentum becomes continuous and we have $\phi_p \in (0, \pi)$. Writing H^{iKSEA} in the basis, $\{|0\rangle, a_p^\dagger a_{-p}^\dagger |0\rangle, a_p^\dagger |0\rangle, a_{-p}^\dagger |0\rangle\}$, we have

$$\bar{H}_p^{iKSEA} = \begin{bmatrix} -h & -(\gamma + K) \sin \phi_p & 0 & 0 \\ (\gamma - K) \sin \phi_p & 2 \cos \phi_p + h & 0 & 0 \\ 0 & 0 & \cos \phi_p & 0 \\ 0 & 0 & 0 & \cos \phi_p \end{bmatrix}. \quad (8)$$

The Hamiltonian in Eq. (8) can be written as $\bar{H}_p^{iKSEA} = \hat{A}_p^\dagger H_p^{iKSEA} \hat{A}_p$, where \hat{A}_p is the column vector, $(a_{-p}^\dagger, a_p)^\dagger$, also known as Nambu spinor [83], and

$$H_p^{iKSEA} = \begin{bmatrix} -h - \cos \phi_p & -(\gamma + K) \sin \phi_p \\ (\gamma - K) \sin \phi_p & \cos \phi_p + h \end{bmatrix}. \quad (9)$$

The eigenvalues of this model are $E_p^{iKSEA} = \pm \epsilon_p$, where

$$\epsilon_p = \sqrt{(h + \cos \phi_p)^2 - (\gamma^2 - K^2) \sin^2 \phi_p}. \quad (10)$$

Depending upon the values of γ and K , two separate regions emerge (see Fig. 2).

Region-I: $\gamma > K$. In this region, we first notice that the second term in Eq. (10) is positive, and hence when it dominates over the first term, the system can have imaginary eigenspectrum. To determine the exceptional point, by calculating $\frac{\partial \epsilon_p}{\partial \phi_p} = 0$ and $\epsilon_p = 0$ from Eq. (10), we obtain the exceptional point, $h_{ep} = \sqrt{1 + \gamma^2 - K^2}$. Note that the exceptional point for the iXY model with $K = 0$ is $\sqrt{1 + \gamma^2}$ which is obtained in the previous study [62]. On the other hand, if we consider the Hermitian KSEA model [74] where we replace $i\gamma$ by γ , the Hamiltonian reads as

$$\begin{aligned} H^{KSEA} = & \sum_j \frac{(1 + \gamma)}{4} \sigma_j^x \sigma_{j+1}^x + \frac{(1 - \gamma)}{4} \sigma_j^y \sigma_{j+1}^y \\ & + \frac{K}{4} (\sigma_j^x \sigma_{j+1}^y + \sigma_j^y \sigma_{j+1}^x) + \frac{h}{2} \sigma_j^z. \end{aligned} \quad (11)$$

By applying the similar procedure as described above, the energy eigenvalues can be obtained as $E_p^{KSEA} =$

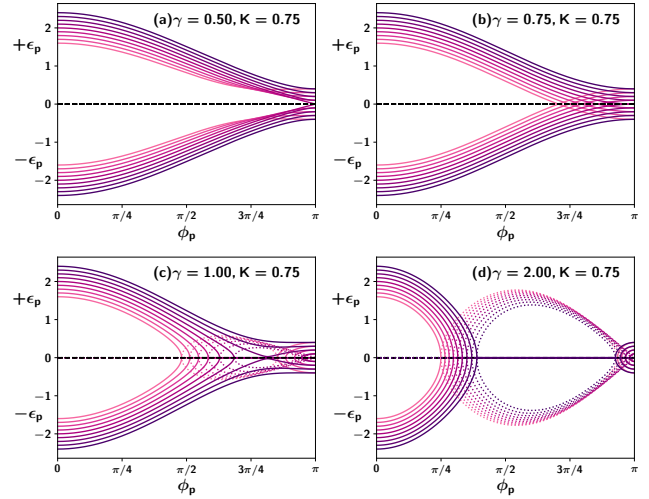


FIG. 2. Energy, $\pm \epsilon_p$ (ordinate) of the $iKSEA$ model against ϕ_p . (a) and (b). $\gamma \leq K$, i.e., Hermitian KSEA interactions dominates over non-Hermiticity parameter while in (c) and (d), the opposite picture is considered with $\gamma > k$. Different lines represent different strength of the magnetic field, 0.6 (lightest) $\leq h \leq 1.4$ (darkest). Solid and dotted lines indicate real and imaginary energies respectively. All axes are dimensionless.

$\pm \sqrt{(h + \cos \phi_p)^2 + (\gamma^2 + K^2) \sin^2 \phi_p}$ [84]. It can be shown that the ground state of the Hamiltonian is a fully product state having vanishing bipartite and multipartite entanglement where $h_f^{KSEA} = \sqrt{1 - \gamma^2 - K^2}$ (see Appendix. B) known as the factorization surface. Hence, the surface of EP is connected to the factorization surface if the non-Hermiticity parameter is changed to imaginary to make the Hamiltonian Hermitian [85].

Region-II: $\gamma \leq K$. In this situation, the second terms is always non-positive and therefore, there exists no momentum block where the model possesses complex eigenvalues. This sector is \mathcal{RT} -symmetry protected without having a broken-to-unbroken transition.

However, the model has different characteristics with the variation of the strength of the magnetic field. Specifically, analyzing Eq. (10), we observe that the extremum momenta (i.e., $\phi_p = \pi$) indicates a quantum critical point at $h_c = 1$. This is the typical second-order quantum phase transition (QPT) [86] that is observed in the transverse XY model in the Hermitian domain. As reported for the Hermitian XY -model, we will now show that bipartite entanglement is capable to identify criticalities in the non-Hermitian model too. It is important to stress here that the computation of bipartite entanglement for this model requires more careful treatment than its Hermitian counterpart as will illustrated in the succeeding section.

III. IDENTIFYING CRITICALITIES VIA BIPARTITE ENTANGLEMENT

The variation of classical correlations between arbitrary two sites with the driving parameter of the Hamiltonian is historically used to signal the transition between phases at zero-temperature of the Hermitian systems. Around two decades ago, it was shown that nearest-neighbor quantum correlations, specifically entanglement can also determine the quantum critical point. In this respect, our contribu-

tion here is to establish the power of bipartite entanglement in detecting quantum critical points in non-Hermitian systems. In order to define the bipartite density matrix in the case of a non-Hermitian system, we have to address a certain subtlety. As the Hamiltonian is non-Hermitian, there are right and left eigenvectors corresponding to an eigenvalue. Thus, a density matrix can be defined in many ways including the left and right vectors. However, in this work, we define $\rho = \frac{|R\rangle\langle R|}{\text{Tr}\rho}$ [78], where $|R\rangle$ is the right eigenvector of the ground state. In case of calculations of experimentally feasible observables, such a choice is valid since the density matrix becomes Hermitian.

To obtain bipartite entanglement, which we measure using logarithmic negativity (see Appendix. A), we require two-body classical correlators and magnetization. From Eq. (9), we rewrite each block as

$$H_p^{iKSEA} = \hat{A}_p^\dagger V_p^{-1} V_p H_p^{iKSEA} V_p^{-1} V_p \hat{A}_p, \quad (12)$$

where $V_p H_p^{iKSEA} (V_p)^{-1} = \text{diag}(+\epsilon_p, -\epsilon_p)$. We define a new operator, $\hat{\eta} = V_p \hat{A}_p$, which forms the non-Hermitian Bogoliubov basis. The matrix V_p can be established by the right eigenvectors and the non-Hermitian Bogoliubov transformation can be represented as [78]

$$\begin{aligned} \eta_p &= -u_p a_{-p}^\dagger - v_p^\dagger a_p, \\ \text{and } \bar{\eta}_p &= -v_p^2 a_p^\dagger + u_p a_{-p}, \end{aligned} \quad (13)$$

where

$$u_p = \frac{h + \cos \phi_p - \epsilon_p}{\sqrt{M}}, \quad v_p^\dagger = \frac{(\gamma + K) \sin \phi_p}{\sqrt{M}},$$

and

$$v_p^2 = \frac{(\gamma - K) \sin \phi_p}{\sqrt{M}}, \quad (14)$$

with $M = -(h + \cos \phi_p - \epsilon_p)^2 + (\gamma^2 - K^2) \sin^2 \phi_p$ and $\{\eta_p, \bar{\eta}_{p'}\} = \delta_{pp'}$.

Any two-qubit density matrix between site i and j , denoted as ρ_{ij} , can be written as

$$\rho_{ij} = \frac{1}{4} \left(\mathbb{I}_4 + \vec{r} \cdot \vec{\sigma} \otimes \mathbb{I} + \mathbb{I} \otimes \vec{s} \cdot \vec{\sigma} + \sum_{k,l=x,y,z} C_{ij}^{kl} \sigma_i^k \otimes \sigma_j^l \right), \quad (15)$$

where the coefficients of Pauli matrices, $r_i^k = \text{Tr}(\sigma_i^k \rho_i)$ and $s_j^k = \text{Tr}(\sigma_j^k \rho_j)$ determine the magnetization in the x, y , and z -directions with ρ_i being the reduced single-site density matrix of ρ_{ij} and $C_{ij}^{kl} = \text{Tr}(\sigma_i^k \otimes \sigma_j^l \rho_{ij})$ denotes the classical correlators. Due to Wick's theorem, an unbalanced number of fermionic creation and annihilation operators is in $m^x, m^y, C^{yz}, C^{zy}, C^{zx}$ and C^{xz} and they all vanish $\forall i$ and j . Hence ρ_{ij} can be expressed as

$$\rho_{ij} = \frac{1}{4} \left(\mathbb{I}_4 + m^z (\sigma_j^z + \sigma_i^z) + \sum_{k,l} C_{ij}^{kl} \sigma_i^k \otimes \sigma_j^l \right). \quad (16)$$

If $|G\rangle$ is the ground state of the Hamiltonian, $\eta_p |G\rangle = 0$ although $\langle G | \bar{\eta}_p \neq 0$. As discussed in Ref. [78], we observe $\langle G | \eta_p^\dagger = 0$, which is another reason to consider the density matrix as $\rho = \frac{|R\rangle\langle R|}{\text{Tr}\rho}$. Hence, we express a_p and a_p^\dagger in terms of η_p and η_p^\dagger as

$$a_p = -\frac{v_p^{1*} \eta_p + u_p \eta_{-p}^\dagger}{|u_p|^2 + |v_p^1|^2} \quad \text{and} \quad a_{-p} = \frac{v_p^{1*} \eta_{-p} - u_p \eta_p^\dagger}{|u_p|^2 + |v_p^1|^2}. \quad (17)$$

Note that η_p and η_p^\dagger do not obey fermionic anti-commutation rule, and $\langle \eta_p \eta_p^\dagger \rangle = |v_p^1|^2 + |u_p|^2$, where the expectation value is calculated with respect to the ground state. In the thermodynamic limit, all

the non-vanishing classical correlators and magnetization involved in the two-site density matrix of the ground state can be obtained in terms of u_p and $v_p^i (i = 1, 2)$ and are given by

$$\begin{aligned} m^z &= \frac{1}{\pi} \int_0^\pi d\phi_p \Lambda_p, \\ C^{xy} &= C^{yx} = \frac{1}{\pi} \int_0^\pi d\phi_p \Omega_p^+ \sin \phi_p, \\ C^{xx} &= \frac{i}{\pi} \int_0^\pi d\phi_p \Omega_p^- \sin \phi_p + \frac{1}{\pi} \int_0^\pi d\phi_p \Lambda_p \cos \phi_p, \\ C^{yy} &= -\frac{i}{\pi} \int_0^\pi d\phi_p \Omega_p^- \sin \phi_p + \frac{1}{\pi} \int_0^\pi d\phi_p \Lambda_p \cos \phi_p, \\ \text{and } C^{zz} &= (m^z)^2 - C^{xx} C^{yy} + C^{xy} C^{yx}. \end{aligned}$$

Here $\Lambda_p = \frac{|v_p^1|^2 - |u_p|^2}{|v_p^1|^2 + |u_p|^2}$, $\Omega_p^- = \frac{u_p v_p^{1*} - v_p^{1*} u_p}{|v_p^1|^2 + |u_p|^2}$ and $\Omega_p^+ = \frac{v_p^{1*} u_p + u_p v_p^1}{|v_p^1|^2 + |u_p|^2}$. We are now ready to probe Region-I and Region-II from the perspective of nearest-neighbor entanglement of the ground state in the non-Hermitian Hamiltonian, H_p^{iKSEA} .

Region-I ($\gamma > K$). In this scenario, both the broken and the unbroken phases exist in the (h, γ) -plane as discussed before. The ground state is unique in the unbroken phase, and is taken as the tensor product of all the eigenvectors with lowest eigenvalues from each momentum block. On the other hand, in the \mathcal{RT} -symmetry broken regime, the definition of the ground state is ambiguous as the imaginary eigenvalues have no definite ordering. However, the choice of the ground state is made where the eigenvector corresponds to the eigenvalue with the lowest imaginary term. With this convention at hand, we compute nearest-neighbor entanglement, denoted by \mathcal{E} quantified via logarithmic negativity [87], of the ground state by varying both h and γ as depicted in Fig. 3. The (γ, h) -plane in this region contains two transition points – (1) exceptional point, where eigenvectors coalesce and cannot exist in Hermitian models, and (2) quantum critical point in which gap-closing happens. Interestingly, non-vanishing bipartite entanglement changes its curvature (see Fig. 4(a)) in both the points. Specifically, for a fixed non-Hermiticity parameter which dominates over the Hermitian KSEA interaction, the first derivative of bipartite entanglement with respect to the magnetic field shows nonanalytic behavior in both the points (as shown in Fig. 4(c)), thereby establishing two kinds of critical points by nature, present in the non-Hermitian models.

Region-II ($\gamma \leq K$). The ground state in this domain possesses two interesting characteristics with the variation of γ and h – (1) critical point at $h_c = 1$ and (2) factorization surface. Notice that the system is quite similar to the transverse XY model in the Hermitian case although there are some stark differences. Specifically, for a fixed non-Hermiticity parameter, bipartite entanglement first decreases with the change of the magnetic field, vanishes at the factorization surface, $h_f = \sqrt{1 + \gamma^2 - K^2}$ and then starts increasing with the increase of h till it reaches its maximal value. Importantly, $\frac{\partial \mathcal{E}}{\partial h}$ again shows kink (non-analyticity) at the gap-closing point $h_c = 1$.

Factorization surface. We report here the factorization surface for the non-Hermitian model, which is well-studied in the Hermitian system [75, 76]. In particular, we find $\mathcal{E} = 0$ at $h_f = \sqrt{1 + \gamma^2 - K^2}$ which is different from factorization surface, known in the Hermitian model, given by $h_f^{\text{herm}} = \sqrt{1 - \gamma^2 - K^2}$. Interestingly, when $K = 0$, the non-Hermitian iXY model in the presence of uniform as well as alternating magnetic fields does not contain factorization surface, thereby illustrating the significance of having $KSEA$ interaction in the non-Hermitian system. Moreover, at $\gamma = K$, $\mathcal{E} = 0 \forall h \geq 1$.

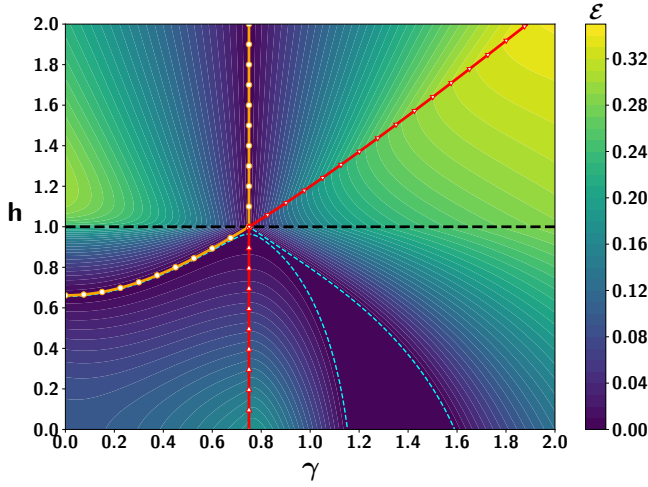


FIG. 3. Contour plot of nearest-neighbor entanglement against external magnetic field, h (vertical axis) and non-Hermiticity parameter, γ (horizontal axis) of the spin chain with both non-Hermitian XY and Hermitian KSEA interactions, given in Eq. (1). Here we set $K = 0.75$ and $N = 5000$. Triangles and circles represent the exceptional points and factorization surface respectively. All axes are dimensionless.

The behavior of the nearest-neighbor entanglement in this region can be explained from another perspective. Let us consider a gauge transformation of the fermionic operators such that

$$c_j = e^{\mu/2} e^{i\theta/2} \bar{c}_j, \quad \text{and} \quad \bar{c}_j = e^{-\mu/2} e^{-i\theta/2} c_j^\dagger, \quad (18)$$

where $e^\mu = \sqrt{\frac{K-\gamma}{K+\gamma}}$ and $\theta = -\pi/2$ with $\{c_j, \bar{c}_k\} = \delta_{jk}$. According to this transformation, we can re-express Eq. (6) as

$$H_{XY}^{JW} = \frac{1}{2} \sum_j (\bar{c}_j c_{j+1} + \bar{c}_{j+1} c_j) + \gamma' (\bar{c}_j \bar{c}_{j+1} + c_{j+1} c_j) + h(2\bar{c}_j c_j - 1), \quad (19)$$

where $\gamma' = \sqrt{K^2 - \gamma^2}$. This is the free-fermionic version of the Hermitian XY spin model with transverse magnetic field. The factorization surface of the XY-spin model, $h_f^{XY} = \sqrt{1 - \gamma'^2}$ [75, 76]. Interestingly, it coincides with the factorization surface, $h_f = \sqrt{1 + \gamma^2 - K^2}$ of the non-Hermitian iKSEA in the unbroken region. Via the mapping in Eq. (18), we can obtain a justification for the similar behavior of nearest-neighbor entanglement in the iKSEA model in this unbroken region and the transverse XY model. The entire analysis establishes that even for the non-Hermitian system, bipartite entanglement can be a good indicator to identify all kinds of transitions, ranging from gap-closing of the energy spectrum, coalescence of eigenvectors, to vanishing entanglement surface. More ambitiously, in the succeeding section, we probe how entanglement is capable to detect these transitions even under quenching.

IV. DYNAMICAL BEHAVIOR: LOSCHMIDT ECHO AND ENTANGLEMENT

Non-Hermitian systems naturally occur under dissipative dynamics of a larger Hermitian system undergoing unitary evolution. Thus

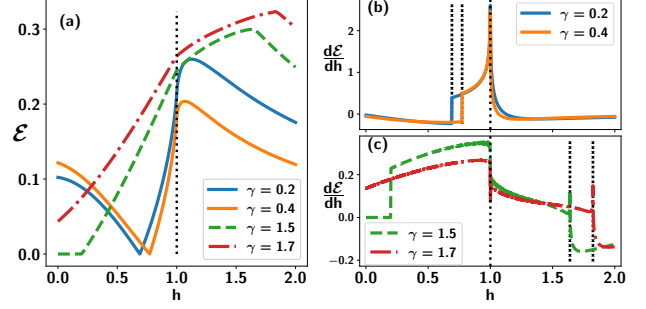


FIG. 4. **Variation of nearest-neighbor entanglement, \mathcal{E} (ordinate) as a function of external magnetic field, h (abscissa).** (a) Bipartite entanglement between the nearest neighbor spins for $\gamma < K$ (solid lines) and $\gamma > K$ (dashed and dashed-dotted lines). Other system parameters are $K = 0.75$ and $N = 5000$. (b) Derivative of nearest-neighbor entanglement with h for $\gamma < K$. $\frac{d\mathcal{E}}{dh}$ is non-analytic at the factorization points (light dashed line) and at the critical point $h_c = 1$ (dark dashed line). (c) $\frac{d\mathcal{E}}{dh}$ vs h for $\gamma > K$ which is non-analytic at the exceptional points (light dashed line) and at the critical point, $h_c = 1$ (dark dashed line). All the axes are dimensionless.

it is imperative to study the dynamical behavior of the physical quantities under non-Hermitian evolution. For carrying out such investigations, the set up considered here is as follows:

1. *Initial state preparation.* - The ground state of the Hamiltonian $H_p^{iKSEA}(h_0) = H_p^0$ with magnetic field, h_0 , is chosen to be the initial state which is taken to be the right eigenvector corresponding to the ground state energy, written as $|\Psi'(0)_p\rangle = (-v_p^1, u_p)^T$. In order to detect probability or to construct density matrix, the normalization of the eigenstate of H_p^0 is performed using the standard Dirac inner product [51, 88], i.e, we should consider

$$|\Psi(0)_p\rangle = \frac{|\Psi'(0)_p\rangle}{\sqrt{|v_p^1|^2 + |u_p|^2}}. \quad (20)$$

2. *Dynamics.* - The initial magnetic field, h_0 is suddenly quenched to h_1 at $t > 0$, which leads to the evolution of the system governed by the Hamiltonian, $H_p^{iKSEA}(h_1) = H_p^1$. The time evolved state is written in the momentum block as

$$|\Psi(t)_p\rangle = e^{-iH_p^1 t} |\Psi(t)_p\rangle; \quad |\Psi(t)_p\rangle = \frac{|\Psi(t)_p\rangle}{\| |\Psi(t)_p\rangle \|}, \quad (21)$$

which leads to the evolved state of the system as $|\Psi(t)\rangle = \otimes_P |\Psi(t)_p\rangle$. The idea is to choose h_0 and h_1 across transition lines and study the effects on dynamical quantities like Loschmidt echo, and corresponding the rate function, and entanglement.

A. Mimicking criticalities via rate function and its breakdown

To analyze whether the dynamical properties of the system can reflect the previously established criticalities, the initial state preparation and the quenching are performed in Region - II with $\gamma \leq K$. Before reporting the results, let us define the dynamical quantity, Loschmidt echo (LE), and the corresponding rate function as

$$\mathcal{L}(t) = \frac{\| \langle \Psi(0) | \Psi(t) \rangle \|^2}{\| \langle \Psi(t) | \Psi(t) \rangle \|}, \quad \lambda(t) = -\frac{1}{N} \log \mathcal{L}(t). \quad (22)$$

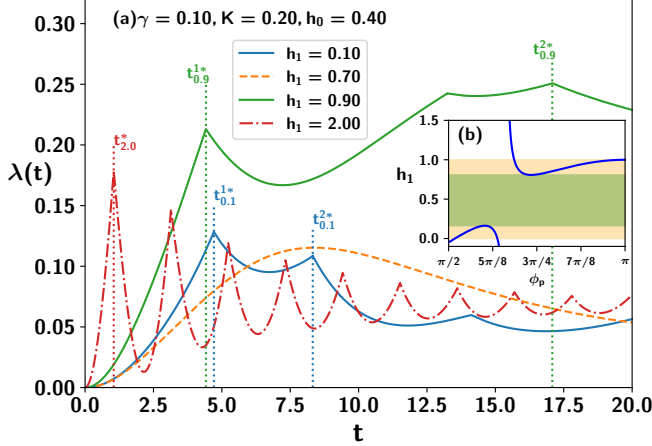


FIG. 5. Rate function, $\lambda(t)$ (vertical axis) as a function of time, t (horizontal axis). (a) From the non-analyticity of $\lambda(t)$, the signature of DQPT is confirmed by quenching in different parameter regimes (dashed-dotted line). However, even when the system is quenched in the same regions, $h_1 = 0.1$, and 0.9 (shown by blue and green solid lines) with the initial ground state, non-analytic rate functions are found although such non-analytic behavior is absent for $h_1 = 0.7$ (dashed line). Other system parameters are $\gamma = 0.1$, $K = 0.2$, $h_0 = 0.4$ and $N = 5000$. (b) DQPT condition on quenched parameter, h_1 . When the curve of h_1 lies in the green (dark shaded) region, no DQPT occurs while when it crosses the yellow (light shaded) region, it shows DQPT without crossing the critical lines. Critical times are mentioned in the graph as $t_{h_1}^*$. All the axes are dimensionless.

Both quantities calculated in the dynamics correspond to dynamical free energy, and their non-analyticities with time have been shown to signal equilibrium quantum phase transition efficiently for Hermitian systems [34, 36] (for exceptions, see Refs. [39, 89–91]).

The Loschmidt echo (LE) for the iKSEA model takes the form as

$$\mathcal{L}(t) = \prod_p \left\| \cos \epsilon_p^1 t - i \langle \psi(0) | H_p^1 | \psi(0) \rangle \frac{\sin \epsilon_p^1 t}{\epsilon_p^1} \right\|^2, \quad (23)$$

where ϵ_p^1 is the energy of the quenched Hamiltonian, H_p^1 . First note that LE vanishes, when ϵ_p^1 is only real, i.e., when the quenching is done by the Hamiltonian in the unbroken phase. This keeps both $\cos \epsilon_p^1 t$ and $\frac{\sin \epsilon_p^1 t}{\epsilon_p^1}$ terms always real.

In the thermodynamic limit, there exists a momentum, $\phi_{p_c} \in (0, \pi)$ such that $\langle \psi(0) | H_{p_c}^1 | \psi(0) \rangle = 0$ which provides a necessary and sufficient condition for LE to become zero and implies that DQPT occurs. Preparing the ground state of the Hamiltonian with the local magnetic field, h_0 and quenching to h_1 , the relation in terms of γ and K ($\gamma < K$) is given by

$$h_1 = h_0 + \epsilon_{p_c}^0 \frac{(h_0 + \cos \phi_{p_c} - \epsilon_{p_c}^0)^2 + (\gamma + K)^2 \sin^2 \phi_{p_c}}{(h_0 + \cos \phi_{p_c} - \epsilon_{p_c}^0)^2 - (\gamma + K)^2 \sin^2 \phi_{p_c}}, \quad (24)$$

where $\epsilon_{p_c}^0$ is the initial energy at critical momenta. It leads to the critical time for DQPT as $t_n^* = \frac{\pi}{\epsilon_{p_c}^1} (n + \frac{1}{2})$, ($n \in \mathbb{Z}$), where $\epsilon_{p_c}^1 = \sqrt{(h + \cos \phi_{p_c})^2 - (\gamma^2 - K^2) \sin^2 \phi_{p_c}}$.

This shows that when the initial and quenching Hamiltonian is taken with h_0 and h_1 respectively having $\gamma \leq K$, DQPT occurs if

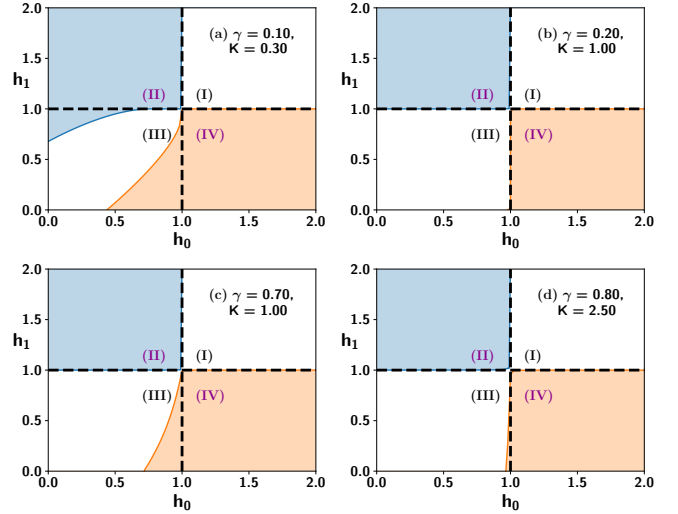


FIG. 6. **Non-analyticities of the rate function in the (h_0, h_1) -plane** for different pairs of γ and K values. The entire region is divided into four quadrants – QI and QIII corresponds to initial and quenching magnetic fields without crossing the critical line $h_c = 1$, while the quadrants, QII and QIV requires the crossing of the critical line. Rate functions correctly detect QII and QIV regions, thereby efficiently identifying DQPT although the incorrect signals are given by the rate function when the system parameters are tuned in QIII. Notice, however, that when both the initial and quenched magnetic fields are above unity, the rate function does not show any non-analyticity. Other parameters of the system is presented in the legend. All axes are dimensionless.

and only if there exists a critical momentum $\phi_{p_c} \in (0, \pi)$, so that h_1 satisfies Eq. (24). Using this condition, we prove that LE obtained via quenching dynamics cannot always mimic the transition which are present as shown in Fig. 5(a).

To examine more precisely, we analyze for several initial states and final quenches in the (h_0, h_1) -plane for a fixed γ and K . Specifically, we divide the entire (h_0, h_1) -plane in four quadrants, namely QI ($1 < h_0 < 2, 1 < h_1 < 2$), QII ($0 < h_0 < 1, h_1 > 1$), QIII ($0 < h_0 < 1, 0 < h_1 < 1$), and QIV ($h_0 > 1, 0 < h_1 < 1$) for identifying $h_c = 1$ in dynamics. The quadrant I and III correspond to quench in which no critical line is crossed for initial and quenched Hamiltonian while the other two quadrants represent the scenario with the initial and the final states being taken across the critical lines. For an ideal DQPT signature, the rate function should not be nonanalytic in the QI and QIII regions. However, in Fig. 6, this is not the case. Although the rate function can faithfully distinguish the situation when the quenching is performed across the critical line as depicted for QII and QIV, there are pairs of (K, γ) values where non-analyticities in the rate function is observed in QIII. Another interesting finding is that the rate function never becomes non-analytic when both the magnetic fields, h_0 and h_1 are strong i.e., $(h_0, h_1) > h_c \equiv 1$. Moreover, we find that there are two critical momenta which correspond to two different critical times when $0 < h_0 < 1$ and $0 < h_1 < 1$ while a unique time is obtained when $h_0 < 1$ and $h_1 > 1$ (QII) or $h_0 > 1$ and $h_1 < 1$ (QIV) (as shown in Fig. 5(b)). This is the reason behind the non-analytic behavior of the rate function seen in different quadrants including the false signature.

After visualizing the picture with respect to the variation of h_0 and h_1 , let us focus on the role of γ and K in finding non-analyticities

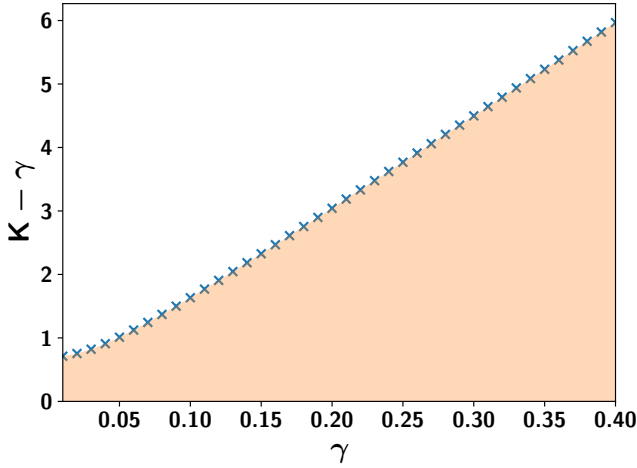


FIG. 7. Conditions on K and γ for dynamical phase transition mimicking the critical lines. Crosses separate the region in two sectors – shaded portion corresponds to the region in which non-analyticity in the rate function incorrectly identify the quenching and the initial magnetic field regimes (same as QIII in Fig. 6) while the rate function detects DQPT in the white portion only when the critical line is crossed. Both the axes are dimensionless.

in the rate function with respect to the quenching in the magnetic field. Note that the values of γ represent the non-Hermiticity amount in the model while with high K values, the system approaches the Hermitian one. Our careful analysis reveals that the wrong signal by the rate function is obtained when γ dominates over K . The rate function can correctly signal the crossing of critical lines during the quench when the difference between K and γ increases (see Fig. 7) for depiction).

B. Determination of criticalities via fluctuation of dynamical entanglement

In Hermitian systems, nearest-neighbor entanglement is shown to be capable of detecting equilibrium phase transition occurring at zero-temperature and dynamical quantum phase transition [92–96]. Let us examine how bipartite entanglement is effective in the case of the non-Hermitian model. Without the evolution, we have already shown in Sec. III that the critical points including exceptional points can be identified via the patterns of bipartite entanglement. We are interested to study the behavior of nearest-neighbor entanglement $\mathcal{E}(t)$ with the variation of time. We observe that the fluctuation pattern of entanglement can discriminate the quadrants mentioned in Fig. 6 for a fixed non-Hermiticity parameter γ and the KSEA strength K . To quantify such an effect, we introduce a quantity,

$$\sigma_{\mathcal{E}} = \lim_{t \rightarrow \infty} \sqrt{\langle \mathcal{E}(t)^2 \rangle_t - \langle \mathcal{E}(t) \rangle_t^2}, \quad (25)$$

as the figure of merit to detect quantum critical points using dynamical entanglement. Let us summarise the result according to four quadrants in Fig. 6. In particular, in the first quadrant QI, $\sigma_{\mathcal{E}}$ is very low and is not sensitive to the change of initial magnetic field, h_0 while when the system parameters are tuned in QIV, $\sigma_{\mathcal{E}}$ is comparatively high although it does not vary with the initial magnetic field

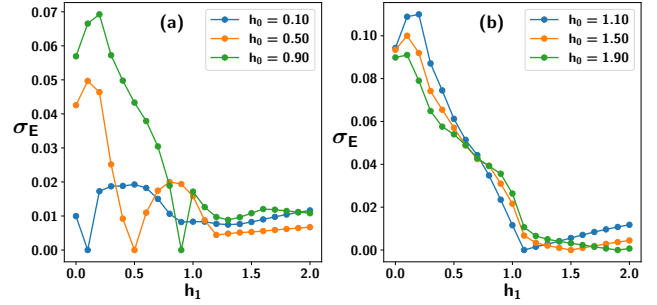


FIG. 8. Fluctuations in the dynamics of nearest-neighbor entanglement (ordinate), quantified via $\sigma_{\mathcal{E}}$, defined in Eq. (25) against the strength of the magnetic field in the quenching Hamiltonian, h_1 (abscissa). Here $\gamma = 0.5, K = 1$, with $N = 2000$. (a). The initial magnetic fields are chosen below the critical line. Note that the left portion till $h_1 = 1$ corresponds to the QIII while the parameters belong to QII when $h_1 > 1$. (b). h_0 is below the critical point, $h_c = 1$ and it covers the QI and QIV. Both the axes are dimensionless.

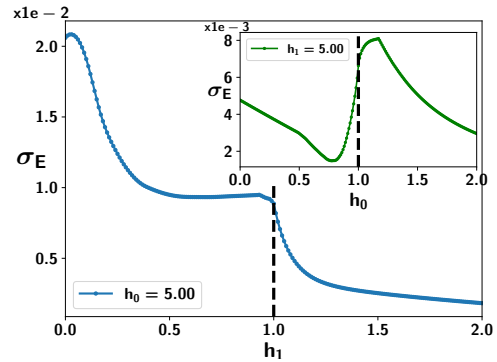


FIG. 9. $\sigma_{\mathcal{E}}$ (ordinate) vs h_1 (abscissa) for a fixed value of $h_0 = 5$. All other specifications are same as in Fig. 8. (Inset) It is similar to the main figure except we interchange h_0 and h_1 , i.e., the quenching magnetic field is fixed to $h_1 = 5$ and the behavior of $\sigma_{\mathcal{E}}$ is plotted with respect to h_0 . Clearly, $\sigma_{\mathcal{E}}$ determines the critical point, $h_c = 1$. Both the axes are dimensionless.

h_0 (as shown in Fig. 8(b)). On the other hand, $\sigma_{\mathcal{E}}$ is extremely sensitive with the choice of the initial magnetic field h_0 in the QIII region. In QII, the fluctuations of entanglement are small irrespective of the values of h_0 (as shown in Fig. 8(a)). The signature of criticality from $\sigma_{\mathcal{E}}$ becomes prominent when $h_0 \gg h_c$ or $h_1 \gg h_c$, i.e., in the domain of QI and QIV (see Fig. 9). In particular, when $h_1 < h_c$, $\sigma_{\mathcal{E}}$ is high and then saturates near $h_c = 1$ while it suddenly changes its curvature when $h_1 > h_c$ with $h_0 \gg h_c$. Similar behavior also emerges when the final quenching magnetic field is also very strong and the initial field is varying as depicted in the inset of Fig. 9.

V. CONCLUSION

Non-Hermitian many-body systems which can be obtained from Hermitian systems connected with an environment, can reveal some exquisite features, typically absent in their Hermitian counterparts. In particular, along with the critical points where the gap between

eigenenergies vanishes, the non-Hermiticity leads to an exceptional point where eigenvectors coalesce and it divides the system into two phases, broken and unbroken regimes.

To explore the non-Hermitian system, we investigated a system containing \mathcal{RT} -symmetric iXY having imaginary non-Hermiticity parameter and Hermitian Kaplan-Shekhtman-Entin-Aharony (KSEA) interactions along with the transverse magnetic field. We realize that when a XX spin chain with KSEA interaction is in contact with local and non-local baths, the effective Hamiltonian represents the non-Hermitian model studied in this work. We found that there is a trade-off relation between the strength of non-Hermiticity and Hermitian KSEA interaction strength. In particular, by exploiting the Jordan-Wigner transformation, we identified that the system possesses three interesting transitions – exceptional points dividing the broken-unbroken region, factorization point having vanishing entanglement in the ground state, and the critical point where the energy gap vanishes in the transverse magnetic field line. We report that the nearest-neighbor entanglement can determine all these points successfully. To our knowledge, the factorization surface in the non-Hermitian model has never been determined in the literature.

Starting from the ground state of the model, we observed that both the rate function and bipartite entanglement can capture the situation when the quenching Hamiltonian is in a different domain than the initial Hamiltonian. However, there are regimes where the rate function can signal the criticality incorrectly. In the case of bipartite entanglement in the evolved state, we found that the fluctuations quantified by the second moment of nearest-neighbor entanglement after averaging over a long time can accurately predict the criticalities present in the model. Our investigations establish that entanglement is competent to determine both Hermitian and non-Hermitian properties of a many-body system.

ACKNOWLEDGEMENTS

We acknowledge the support from Interdisciplinary Cyber Physical Systems (ICPS) program of the Department of Science and Technology (DST), India, Grant No.: DST/ICPS/QuST/Theme-1/2019/23. We acknowledge the use of **QIClib** – a modern C++ library for general purpose quantum information processing and quantum computing (<https://titaschanda.github.io/QIClib>) and cluster computing facility at Harish-Chandra Research Institute.

Appendix A: Logarithmic Negativity

We quantify entanglement in two-qubit systems by logarithmic-negativity (LN). For a given bipartite state ρ_{ij} between two node, i and j , LN [87, 97, 98] is defined as

$$\mathcal{E}(\rho_{ij}) = \log_2(2\mathcal{N}(\rho_{ij}) + 1),$$

$$\delta = \min_{\alpha^{e(o)}, \beta^{e(o)}} \frac{K}{4} \{ \sin \alpha^e \sin \alpha^o \sin(\beta^e + \beta^o) \} + \frac{1}{4} \{ h(\cos \alpha^e + \cos \alpha^o) + (\cos(\beta^e - \beta^o) + \gamma \cos(\beta^e + \beta^o)) \sin \alpha^e \alpha^o \} \quad (\text{B6})$$

After performing minimization over the real parameters of $\alpha^{e(o)}$ and $\beta^{e(o)}$, the optimum value of δ is obtained for

$$\begin{aligned} \beta^e = \beta^o = \beta &= \frac{1}{2} \arctan \frac{K}{\gamma}, \\ \alpha^e &= \arccos \left(\frac{1}{\omega} \right), \\ \text{and } \alpha^o &= \arctan \left(\sqrt{\omega^2 - 1} \right), \end{aligned} \quad (\text{B7})$$

where \mathcal{N} is the absolute sum of negative eigenvalues of the partially transposed state ($\rho_{ij}^{T_i}$ or $\rho_{ij}^{T_j}$) with partial transposition being taken with respect to either i or j .

Appendix B: Factorization surface of KSEA model

Let us derive the factorization surface for the Hermitian KSEA model which is described as

$$\begin{aligned} H^{KSEA} &= \sum_j \frac{(1+\gamma)}{4} \sigma_j^x \sigma_{j+1}^x + \frac{(1-\gamma)}{4} \sigma_j^y \sigma_{j+1}^y \\ &+ \frac{K}{4} (\sigma_j^x \sigma_{j+1}^y + \sigma_j^y \sigma_{j+1}^x) + \frac{h}{2} \sigma_j^z, \end{aligned} \quad (\text{B1})$$

where $\sigma_{N+1} = \sigma_1$. Due to periodic boundary condition(PBC), the separable state at the factorization point can be written as

$$|\Phi\rangle = \prod_{j=0}^{N/2-1} |\phi_{2j}^e\rangle \otimes |\phi_{2j+1}^o\rangle, \quad (\text{B2})$$

where $|\phi^{(o)e}\rangle$ are the state at odd (even) site. The Hamiltonian can be written by dividing into odd and even sector as $H^{KSEA} = \sum_j^{N/2-1} (H_{2j,2j+1}^{eo} + H_{2j+1,2j+2}^{oe})$ where H^{eo} is a two-site Hamiltonian given by the form,

$$\begin{aligned} H^{eo} &= \frac{(1+\gamma)}{4} \sigma_e^x \sigma_o^x + \frac{(1-\gamma)}{4} \sigma_e^y \sigma_o^y + \frac{h}{4} \sigma_e^z + \frac{h}{4} \sigma_o^z \\ &+ \frac{K}{4} (\sigma_e^x \sigma_o^y + \sigma_e^y \sigma_o^x). \end{aligned} \quad (\text{B3})$$

We have to show that $|\Phi\rangle$ is the eigenstate of the H^{KSEA} corresponding to the minimum energy and the parameter space has to be identified which leads to the ground state H^{KSEA} . Let us compute the minimum energy obtained from H^{KSEA} via H^{KSEA} where the minimization is performed over the set of product states, i.e.,

$$\begin{aligned} E_{min} &= \min_{|\phi^e\rangle|\phi^o\rangle} \langle \Phi | H^{KSEA} | \Phi \rangle \\ &= N \min_{|\phi^e\rangle|\phi^o\rangle} \langle \phi^e | \langle \phi^o | H^{eo} | \phi^e \rangle | \phi^o \rangle, \end{aligned} \quad (\text{B4})$$

where we have used the fact that H^{eo} and H^{oe} are energetically equivalent. Hence, the minimization depends upon the separable energy per site which is $\delta = \min_{|\phi^e\rangle|\phi^o\rangle} \langle \phi^e | \langle \phi^o | H^{eo} | \phi^e \rangle | \phi^o \rangle$ and the states, $|\phi^{(o)e}\rangle$ is, in general can be written as

$$|\phi^{(o)e}\rangle = \cos \frac{\alpha^{e(o)}}{2} |0\rangle + \exp(i\beta^{e(o)}) \sin \frac{\alpha^{e(o)}}{2} |1\rangle, \quad (\text{B5})$$

where $0 \leq \alpha^{e(o)} \leq \pi$ and $0 \leq \beta^{e(o)} \leq 2\pi$. The minimum energy, δ is re-expressed as

where $\omega = (K \sin 2\beta + \gamma \cos 2\beta + 1)/h$. It shows that $|\Phi\rangle$ is the ground state of the Hamiltonian if $\delta = \delta_g$ where $\delta_g = -\frac{1}{2} \sqrt{h^2 + K^2 + \gamma^2}$ is the energy of ground state of H^{eo} . This

leads to the equation of factorization surface, which depends on the

Hamiltonian parameters,

$$h^2 = 1 - \gamma^2 - K^2. \quad (\text{B8})$$

-
- [1] Z. Gong, Y. Ashida, K. Kawabata, K. Takasan, S. Higashikawa, and M. Ueda, Topological phases of non-hermitian systems, *Phys. Rev. X* **8**, 031079 (2018).
- [2] K. Kawabata, K. Shiozaki, M. Ueda, and M. Sato, Symmetry and topology in non-hermitian physics, *Phys. Rev. X* **9**, 041015 (2019).
- [3] C. Chen, L. Jin, and R.-B. Liu, Sensitivity of parameter estimation near the exceptional point of a non-hermitian system, *New Journal of Physics* **21**, 083002 (2019).
- [4] U. Günther and B. F. Samsonov, \mathcal{PT} -symmetric brachistochrone problem, lorentz boosts, and nonunitary operator equivalence classes, *Phys. Rev. A* **78**, 042115 (2008).
- [5] D. C. Brody and E.-M. Graefe, Mixed-state evolution in the presence of gain and loss, *Phys. Rev. Lett.* **109**, 230405 (2012).
- [6] S. Liu, S. Ma, C. Yang, L. Zhang, W. Gao, Y. J. Xiang, T. J. Cui, and S. Zhang, Gain- and loss-induced topological insulating phase in a non-hermitian electrical circuit, *Phys. Rev. Appl.* **13**, 014047 (2020).
- [7] H.-P. Breuer and F. Petruccione, *The Theory of Open Quantum Systems* (2006).
- [8] D. A. Lidar, Lecture notes on the theory of open quantum systems (2020), [arXiv:1902.00967 \[quant-ph\]](https://arxiv.org/abs/1902.00967).
- [9] T. Ohlsson and S. Zhou, Density-matrix formalism for \mathcal{PT} -symmetric non-hermitian hamiltonians with the lindblad equation, *Phys. Rev. A* **103**, 022218 (2021).
- [10] S. Khandelwal, N. Brunner, and G. Haack, Signatures of liouvilian exceptional points in a quantum thermal machine, *PRX Quantum* **2**, 040346 (2021).
- [11] W. Chen, M. Abbasi, B. Ha, S. Erdamar, Y. N. Joglekar, and K. W. Murch, Decoherence-induced exceptional points in a dissipative superconducting qubit, *Phys. Rev. Lett.* **128**, 110402 (2022).
- [12] Y. Nakanishi and T. Sasamoto, \mathcal{PT} phase transition in open quantum systems with lindblad dynamics, *Phys. Rev. A* **105**, 022219 (2022).
- [13] F. Minganti, A. Miranowicz, R. W. Chhajlany, I. I. Arkhipov, and F. Nori, Hybrid-liouvillian formalism connecting exceptional points of non-hermitian hamiltonians and liouvillians via postselection of quantum trajectories, *Phys. Rev. A* **101**, 062112 (2020).
- [14] C. Fleckenstein, A. Zorzato, D. Varjas, E. J. Bergholtz, J. H. Bardarson, and A. Tiwari, Non-hermitian topology in monitored quantum circuits, *Phys. Rev. Res.* **4**, L032026 (2022).
- [15] Ş. K. Özdemir, S. Rotter, F. Nori, and L. Yang, Parity–time symmetry and exceptional points in photonics, *Nature Materials* **18**, 783 (2019).
- [16] W. Chen, M. Abbasi, Y. N. Joglekar, and K. W. Murch, Quantum jumps in the non-hermitian dynamics of a superconducting qubit, *Phys. Rev. Lett.* **127**, 140504 (2021).
- [17] T. K. Konar, L. G. C. Lakkaraju, and A. S. De, Quantum battery with non-hermitian charging (2022), [arXiv:2203.09497 \[quant-ph\]](https://arxiv.org/abs/2203.09497).
- [18] P. Djourwe, Y. Pennec, and B. Djafari-Rouhani, Exceptional point enhances sensitivity of optomechanical mass sensors, *Phys. Rev. Appl.* **12**, 024002 (2019).
- [19] C. Chen, L. Jin, and R.-B. Liu, Sensitivity of parameter estimation near the exceptional point of a non-hermitian system, *New Journal of Physics* **21**, 083002 (2019).
- [20] H.-K. Lau and A. A. Clerk, Fundamental limits and non-reciprocal approaches in non-hermitian quantum sensing, *Nature Communications* **9**, 4320 (2018).
- [21] H. Hodaei, A. U. Hassan, S. Wittek, H. Garcia-Gracia, R. El-Ganainy, D. N. Christodoulides, and M. Khajavikhan, Enhanced sensitivity at higher-order exceptional points, *Nature* **548**, 187 (2017).
- [22] M. Am-Shallem, R. Kosloff, and N. Moiseyev, Exceptional points for parameter estimation in open quantum systems: analysis of the bloch equations, *New Journal of Physics* **17**, 113036 (2015).
- [23] W. Chen, Ş. Kaya Özdemir, G. Zhao, J. Wiersig, and L. Yang, Exceptional points enhance sensing in an optical microcavity, *Nature* **548**, 192 (2017).
- [24] M. Naghiloo, M. Abbasi, Y. N. Joglekar, and K. W. Murch, Quantum state tomography across the exceptional point in a single dissipative qubit, *Nature Physics* **15**, 1232 (2019).
- [25] Y. Ashida, Z. Gong, and M. Ueda, Non-hermitian physics, *Advances in Physics* **69**, 249 (2020), <https://doi.org/10.1080/00018732.2021.1876991>.
- [26] M. Abbasi, W. Chen, M. Naghiloo, Y. N. Joglekar, and K. W. Murch, Topological quantum state control through exceptional-point proximity, *Phys. Rev. Lett.* **128**, 160401 (2022).
- [27] C. M. Bender and S. Boettcher, Real spectra in non-hermitian hamiltonians having \mathcal{PT} symmetry, *Phys. Rev. Lett.* **80**, 5243 (1998).
- [28] D. C. Brody, Biorthogonal quantum mechanics, *Journal of Physics A: Mathematical and Theoretical* **47**, 035305 (2013).
- [29] F. Minganti, A. Miranowicz, R. W. Chhajlany, and F. Nori, Quantum exceptional points of non-hermitian hamiltonians and liouvillians: The effects of quantum jumps, *Phys. Rev. A* **100**, 062131 (2019).
- [30] A. Mostafazadeh, Pseudo-Hermiticity versus PT symmetry: The necessary condition for the reality of the spectrum of a non-Hermitian Hamiltonian, *Journal of Mathematical Physics* **43**, 205 (2002), https://pubs.aip.org/aip/jmp/article-pdf/43/1/205/7481018/205_1_online.pdf.
- [31] C. M. Bender, D. C. Brody, and H. F. Jones, Complex extension of quantum mechanics, *Phys. Rev. Lett.* **89**, 270401 (2002).
- [32] C. Yang, Y. Wang, P. Wang, X. Gao, and S. Chen, Dynamical signature of localization-delocalization transition in a one-dimensional incommensurate lattice, *Phys. Rev. B* **95**, 184201 (2017).
- [33] R. Hamazaki, K. Kawabata, and M. Ueda, Non-hermitian many-body localization, *Phys. Rev. Lett.* **123**, 090603 (2019).
- [34] M. Heyl, A. Polkovnikov, and S. Kehrein, Dynamical quantum phase transitions in the transverse-field ising model, *Phys. Rev. Lett.* **110**, 135704 (2013).
- [35] M. Heyl, Scaling and universality at dynamical quantum phase transitions, *Phys. Rev. Lett.* **115**, 140602 (2015).
- [36] M. Heyl, Dynamical quantum phase transitions: a review, *Reports on Progress in Physics* **81**, 054001 (2018).
- [37] R. Jafari, Dynamical quantum phase transition and quasi particle excitation, *Scientific Reports* **9**, 2871 (2019).

- [38] R. Jafari, H. Johannesson, A. Langari, and M. A. Martin-Delgado, Quench dynamics and zero-energy modes: The case of the creutz model, *Phys. Rev. B* **99**, 054302 (2019).
- [39] S. Haldar, S. Roy, T. Chanda, A. Sen(De), and U. Sen, Multipartite entanglement at dynamical quantum phase transitions with nonuniformly spaced criticalities, *Phys. Rev. B* **101**, 224304 (2020).
- [40] S. Zamani, R. Jafari, and A. Langari, Floquet dynamical quantum phase transition in the extended xy model: Nonadiabatic to adiabatic topological transition, *Phys. Rev. B* **102**, 144306 (2020).
- [41] U. Mishra, R. Jafari, and A. Akbari, Disordered kitaev chain with long-range pairing: Loschmidt echo revivals and dynamical phase transitions, *Journal of Physics A: Mathematical and Theoretical* **53**, 375301 (2020).
- [42] R. Modak and D. Rakshit, Many-body dynamical phase transition in a quasiperiodic potential, *Phys. Rev. B* **103**, 224310 (2021).
- [43] R. Jafari and A. Akbari, Floquet dynamical phase transition and entanglement spectrum, *Phys. Rev. A* **103**, 012204 (2021).
- [44] M. Sadrzadeh, R. Jafari, and A. Langari, Dynamical topological quantum phase transitions at criticality, *Phys. Rev. B* **103**, 144305 (2021).
- [45] A. Haldar, K. Mallayya, M. Heyl, F. Pollmann, M. Rigol, and A. Das, Signatures of quantum phase transitions after quenches in quantum chaotic one-dimensional systems, *Phys. Rev. X* **11**, 031062 (2021).
- [46] P. Nandi, S. Bhattacharyya, and S. Dasgupta, Detection of quantum phase boundary at finite temperatures in integrable spin models, *Phys. Rev. Lett.* **128**, 247201 (2022).
- [47] J. Naji, M. Jafari, R. Jafari, and A. Akbari, Dissipative floquet dynamical quantum phase transition, *Phys. Rev. A* **105**, 022220 (2022).
- [48] R. Jafari, A. Akbari, U. Mishra, and H. Johannesson, Floquet dynamical quantum phase transitions under synchronized periodic driving, *Phys. Rev. B* **105**, 094311 (2022).
- [49] J. Naji, R. Jafari, L. Zhou, and A. Langari, Engineering floquet dynamical quantum phase transitions, *Phys. Rev. B* **106**, 094314 (2022).
- [50] L. Zhou, Q.-h. Wang, H. Wang, and J. Gong, Dynamical quantum phase transitions in non-hermitian lattices, *Phys. Rev. A* **98**, 022129 (2018).
- [51] X. M. Yang and Z. Song, Resonant generation of a p -wave cooper pair in a non-hermitian kitaev chain at the exceptional point, *Phys. Rev. A* **102**, 022219 (2020).
- [52] D. Mondal and T. Nag, Anomaly in the dynamical quantum phase transition in a non-hermitian system with extended gapless phases, *Phys. Rev. B* **106**, 054308 (2022).
- [53] D. Mondal and T. Nag, Finite temperature dynamical quantum phase transition in a non-hermitian system (2022).
- [54] T. E. Lee, F. Reiter, and N. Moiseyev, Entanglement and spin squeezing in non-hermitian phase transitions, *Phys. Rev. Lett.* **113**, 250401 (2014).
- [55] Z.-X. Guo, X.-J. Yu, X.-D. Hu, and Z. Li, Emergent phase transitions in a cluster ising model with dissipation, *Phys. Rev. A* **105**, 053311 (2022).
- [56] F. Yang, H. Wang, M.-L. Yang, C.-X. Guo, X.-R. Wang, G.-Y. Sun, and S.-P. Kou, Hidden continuous quantum phase transition without gap closing in non-hermitian transverse ising model, *New Journal of Physics* **24**, 043046 (2022).
- [57] C. Li, X. Z. Zhang, G. Zhang, and Z. Song, Topological phases in a kitaev chain with imbalanced pairing, *Phys. Rev. B* **97**, 115436 (2018).
- [58] K. Yamamoto, M. Nakagawa, K. Adachi, K. Takasan, M. Ueda, and N. Kawakami, Theory of non-hermitian fermionic superfluidity with a complex-valued interaction, *Phys. Rev. Lett.* **123**, 123601 (2019).
- [59] L. Herviou, N. Regnault, and J. H. Bardarson, Entanglement spectrum and symmetries in non-Hermitian fermionic non-interacting models, *SciPost Phys.* **7**, 069 (2019).
- [60] Y.-X. Xiao and C. T. Chan, Topology in non-hermitian chern insulators with skin effect, *Phys. Rev. B* **105**, 075128 (2022).
- [61] X. Turkeshi and M. Schiró, Entanglement and correlation spreading in non-hermitian spin chains, *Phys. Rev. B* **107**, L020403 (2023).
- [62] X. Z. Zhang and Z. Song, Non-hermitian anisotropic xy model with intrinsic rotation-time-reversal symmetry, *Phys. Rev. A* **87**, 012114 (2013).
- [63] X. Z. Zhang and Z. Song, Non-hermitian anisotropic xy model with intrinsic rotation-time-reversal symmetry, *Phys. Rev. A* **87**, 012114 (2013).
- [64] C. Li, G. Zhang, X. Z. Zhang, and Z. Song, Conventional quantum phase transition driven by a complex parameter in a non-hermitian \mathcal{PT} -symmetric ising model, *Phys. Rev. A* **90**, 012103 (2014).
- [65] C. Li, G. Zhang, and Z. Song, Chern number in ising models with spatially modulated real and complex fields, *Phys. Rev. A* **94**, 052113 (2016).
- [66] T. A. Kaplan, Single-band hubbard model with spin-orbit coupling, *Zeitschrift für Physik B Condensed Matter* **49**, 313 (1983).
- [67] L. Shekhtman, O. Entin-Wohlman, and A. Aharony, Moriya's anisotropic superexchange interaction, frustration, and dzyaloshinsky's weak ferromagnetism, *Phys. Rev. Lett.* **69**, 836 (1992).
- [68] A. Zheludev, S. Maslov, I. Tsukada, I. Zaliznyak, L. P. Regnault, T. Masuda, K. Uchinokura, R. Erwin, and G. Shirane, Experimental evidence for kaplan–shekhtman–entin-wohlman–aharony interactions in $\text{Ba}_2\text{CuGe}_2\text{O}_7$, *Phys. Rev. Lett.* **81**, 5410 (1998).
- [69] A. Metelmann and A. A. Clerk, Nonreciprocal photon transmission and amplification via reservoir engineering, *Phys. Rev. X* **5**, 021025 (2015).
- [70] M. Keck, D. Rossini, and R. Fazio, Persistent currents by reservoir engineering, *Phys. Rev. A* **98**, 053812 (2018).
- [71] E. Lieb, T. Schultz, and D. Mattis, Two soluble models of an antiferromagnetic chain, *Annals of Physics* **16**, 407 (1961).
- [72] E. Barouch, B. M. McCoy, and M. Dresden, Statistical mechanics of the XY model. i, *Phys. Rev. A* **2**, 1075 (1970).
- [73] E. Barouch and B. M. McCoy, Statistical mechanics of the xy model. ii. spin-correlation functions, *Phys. Rev. A* **3**, 786 (1971).
- [74] H. Fu, M. Zhong, and P. Tong, The effects of ksea interaction on the ground-state properties of spin chains in a transverse field, *The European Physical Journal B* **93**, 80 (2020).
- [75] S. M. Giampaolo, G. Adesso, and F. Illuminati, Theory of ground state factorization in quantum cooperative systems, *Phys. Rev. Lett.* **100**, 197201 (2008).
- [76] S. M. Giampaolo, G. Adesso, and F. Illuminati, Separability and ground-state factorization in quantum spin systems, *Phys. Rev. B* **79**, 224434 (2009).
- [77] K. D. Agarwal, T. K. Konar, L. G. C. Lakkaraju, and A. S. De, Detecting exceptional point through dynamics in non-hermitian systems (2022), [arXiv:2212.12403 \[quant-ph\]](https://arxiv.org/abs/2212.12403).
- [78] T. E. Lee and C.-K. Chan, Heralded magnetism in non-hermitian atomic systems, *Phys. Rev. X* **4**, 041001 (2014).
- [79] J. Chovan, M. Marder, and N. Papanicolaou, Field-induced phase transitions in the helimagnet $\text{Ba}_2\text{CuGe}_2\text{O}_7$, *Phys. Rev. B*

- [88, 064421 \(2013\)](#).
- [80] M. Keck, D. Rossini, and R. Fazio, Persistent currents by reservoir engineering, *Phys. Rev. A* **98**, 053812 (2018).
- [81] Y. Zhang, Y.-Q. Ge, and Y. xi Liu, Simulation of Kitaev model using one-dimensional chain of superconducting qubits and environmental effect on topological states (2023), [arXiv:2302.03834 \[quant-ph\]](#).
- [82] A. Y. Kitaev, Unpaired Majorana fermions in quantum wires, *Physics-Uspekhi* **44**, 131 (2001).
- [83] G. B. Mbeng, A. Russomanno, and G. E. Santoro, The quantum Ising chain for beginners (2020), [arXiv:2009.09208 \[quant-ph\]](#).
- [84] E. Barouch, B. M. McCoy, and M. Dresden, Statistical mechanics of the XY model. i, *Phys. Rev. A* **2**, 1075 (1970).
- [85] L. G. C. Lakkaraju and A. Sen(De), Detection of an unbroken phase of a non-hermitian system via a hermitian factorization surface, *Phys. Rev. A* **104**, 052222 (2021).
- [86] S. Sachdev, *Quantum Phase Transitions*, 2nd ed. (Cambridge University Press, 2011).
- [87] G. Vidal and R. F. Werner, Computable measure of entanglement, *Phys. Rev. A* **65**, 032314 (2002).
- [88] S. Lin and Z. Song, Non-hermitian heat engine with all-quantum-adiabatic-process cycle, *Journal of Physics A: Mathematical and Theoretical* **49**, 475301 (2016).
- [89] S. Vajna and B. Dóra, Disentangling dynamical phase transitions from equilibrium phase transitions, *Phys. Rev. B* **89**, 161105 (2014).
- [90] F. Andraschko and J. Sirker, Dynamical quantum phase transitions and the Loschmidt echo: A transfer matrix approach, *Phys. Rev. B* **89**, 125120 (2014).
- [91] V. Gurarie, Dynamical quantum phase transitions in the random field Ising model, *Phys. Rev. A* **100**, 031601 (2019).
- [92] L. Amico, R. Fazio, A. Osterloh, and V. Vedral, Entanglement in many-body systems, *Rev. Mod. Phys.* **80**, 517 (2008).
- [93] A. Sen(De), U. Sen, and M. Lewenstein, Dynamical phase transitions and temperature-induced quantum correlations in an infinite spin chain, *Phys. Rev. A* **72**, 052319 (2005).
- [94] G. De Chiara and A. Sanpera, Genuine quantum correlations in quantum many-body systems: a review of recent progress, *Reports on Progress in Physics* **81**, 074002 (2018).
- [95] A. E. B. Nielsen, G. Sierra, and J. I. Cirac, Violation of the area law and long-range correlations in infinite-dimensional-matrix product states, *Phys. Rev. A* **83**, 053807 (2011).
- [96] A. Osterloh, L. Amico, G. Falci, and R. Fazio, Scaling of entanglement close to a quantum phase transition, *Nature* **416**, 608 (2002).
- [97] M. Horodecki, P. Horodecki, and R. Horodecki, Separability of mixed states: necessary and sufficient conditions, *Physics Letters A* **223**, 1 (1996).
- [98] A. Peres, Separability criterion for density matrices, *Phys. Rev. Lett.* **77**, 1413 (1996).